RESEARCH ARTICLE

Clinical Evaluation of PET Image Quality as a Function of Acquisition Time in a New TOF-PET/MRI Compared to TOF-PET/CT—Initial Results

Konstantinos G. Zeimpekis,[1] Felipe Barbosa,[1] Martin Hüllner,[1] Edwin ter Voert,[1] Helen Davison,[1] Patrick Veit-Haibach,[1,2] Gaspar Delso[3]

[1]*Department of Nuclear Medicine, University Hospital Zurich, Rämistrasse 100, CH-8091, Zürich, Switzerland*
[2]*Department of Diagnostic and Interventional Radiology, University Hospital Zurich, Zurich, Switzerland*
[3]*GE Healthcare, Waukesha, WI, USA*

Abstract

Purpose: The purpose of this study was to compare only the performance of the PET component between a TOF-PET/CT (henceforth noted as PET/CT) scanner and an integrated TOF-PET/MRI (henceforth noted as PET/MRI) scanner concerning image quality parameters and quantification in terms of standardized uptake value (SUV) as a function of acquisition time (a surrogate of dose). The CT and MR image quality were not assessed, and that is beyond the scope of this study.
Procedures: Five brain and five whole-body patients were included in the study. The PET/CT scan was used as a reference and the PET/MRI acquisition time was consecutively adjusted, taking into account the decay between the scans in order to expose both systems to the same amount of the emitted signal. The acquisition times were then retrospectively reduced to assess the performance of the PET/MRI for lower count rates. Image quality, image sharpness, artifacts, and noise were evaluated. SUV measurements were taken in the liver and in the white matter to compare quantification.
Results: Quantitative evaluation showed strong correlation between PET/CT and PET/MRI brain SUVs. Liver correlation was good, however, with lower uptake estimation in PET/MRI, partially justified by bio-redistribution. The clinical evaluation showed that PET/MRI offers higher image quality and sharpness with lower levels of noise and artifacts compared to PET/CT with reduced acquisition times for whole-body scans while for brain scans there is no significant difference.
Conclusion: The TOF-PET/MRI showed higher image quality compared to TOF-PET/CT as tested with reduced imaging times. However, this result accounts mainly for body imaging, while no significant differences were found in brain imaging.

Key words: Image quality, PET/MRI, PET/CT, Solid-state PET detectors, Time-of-flight, Dose reduction

Introduction

In a clinical world where PET/CT has proven its diagnostic excellence after its introduction roughly a decade ago [1], the recently available integrated PET/MRI imaging can offer

significant additional advances in clinical imaging [2–5]. One of the major questions is whether or not PET/MRI is capable of replacing PET/CT for certain clinical indications and which are those indications.

Building an integrated PET/MRI scanner is a challenge due to the different nature of MR and PET technology. The static magnetic field required for MR interferes with the PET detectors introducing signal distortions and the available space is constrained because the MR bore is narrow.

These challenges are partly overcome by introducing solid-state detectors that enable the placement of the PET ring inside the MR bore, leading to an integrated geometry which makes the scanner field of view (FOV) narrower as well as longer. PET/MRI has shown partly enhanced PET-performance due these new detectors and geometry providing higher sensitivity. However, previously reported whole-body systems based on solid-state detectors did not offer high enough sensitivity and time-of-flight performance and thus still provided inferior image quality compared to standard PET/CT [6]. Another study, although, assessed a dedicated PET brain insert prototype featuring solid-state APD readout and has shown an image quality superior to whole-body PET/CT or PET/MRI in brain imaging [7].

Now a new integrated PET/MRI scanner enabling TOF-PET acquisition [8] with silicon photomultipliers (SiPMs) is available and a comparison of the scanner's PET performance can be made with the gold standard TOF-PET/CT.

The purpose of this study was to evaluate the clinical image quality of standard PET/CT with TOF (time-of-flight) compared to the newly introduced TOF-PET/MRI as a function of acquisition time in brain imaging and body imaging.

Procedures

Patient Population

A total of 10 adult patients (5 brain scans and 5 whole-body scans, mean age 52 years, range 32–75 years; 4 women, 6 men) referred for either staging or restaging/follow-up of various malignant tumors participated in this prospective study. Inclusion criteria were clinically indicated whole-body 2-deoxy-2-[^{18}F]-fluoro-D-glucose ([^{18}F]FDG) PET/CT and willingness to participate in the additional PET/MRI. It is important to stress at this point that for all cases, the PET/CT examination was performed first and the PET/MRI followed next. That is because the PET/CT is the standard clinical procedure while the PET/MRI was used only for research purposes when this study was conducted. Exclusion criteria were claustrophobia, MR-incompatible implanted medical devices (*e.g.*, cardiac pacemakers, insulin pumps, neurostimulators, cochlear implants), possible metallic fragments in the body, or a body habitus that did not fit into the PET/MRI gantry. This study was approved by the Institutional Ethics Committee, and written informed consent was obtained from all patients prior to the procedure.

Acquisition Hardware

A sequential TOF-PET/CT (Discovery 690 PET/CT, GE Healthcare, Waukesha, WI) and SIGNA simultaneous TOF-PET/MRI (Signa PET/MRI, GE Healthcare, Waukesha, WI) were used.

The PET/CT system has a cylindrical geometry, formed by a full ring of 24 detector modules. The PET tomograph consists of LYSO ($Lu_{1.8}Y_{0.2}$ $SiO_5(Ce)$) crystals with dimensions of $4.2 \times 6.3 \times 25$ mm^3. The PET detection unit is a block of 54 (9×6) individual LYSO crystals coupled to a single squared photomultiplier tube with 4 anodes. The TOF timing resolution is around 500 ps. The detector ring has a face-to-face diameter of 81 cm with a transaxial field of view of 70 cm and an axial field of view of 15.7 cm [9].

The TOF-PET/MRI system is a hybrid whole-body scanner (Signa PET/MR, GE Healthcare, Waukesha, WI, USA) combining a 3-T wide-bore MR system with TOF-PET detector rings.

The PET system also has a cylindrical geometry, formed by a full ring of 28 detector modules. The detector ring has a face-to-face diameter of 62 cm, with a transaxial field of view of 60 cm and an axial field of view of 25 cm. The detectors are mounted on a custom radiofrequency body coil, centered inside the MR gradient set of a GE Discovery 750w 3 T MR Scanner. Each detector module is individually shielded and includes control electronics, a liquid-cooling circuit, and a Cartesian array of 45×16 LYSO scintillator crystals, each crystal with dimensions of $3.95 \times 5.3 \times 25$ mm^3 [8], covering roughly 64.5×250.0 mm [10] paired with silicon photomultipliers (SiPMs) using tapered light guides. The TOF performance reported by the manufacturer is <400 ps.

Acquisition Protocol

PET/CT Imaging

Patients fasted for 6 h before being injected with [^{18}F]FDG. The administered dose was 3 MBq/kg if the body weight was less than 85 kg or 3.5 MBq/kg otherwise, with a mean administered activity of 234.6 and 224.4 MBq for brain and whole-body scans, respectively. After an uptake time of 60 min (range 55–80 min), the clinically indicated PET/CT scan was performed according to standard imaging protocols of our hospital. Data was acquired in 3D mode with scan duration of 10 min for the brain scan and 2 min per bed position for the whole-body scan. The low-dose CT (used both for attenuation correction and diagnostic purposes) and regular-dose CT scans were acquired during shallow breathing. Scan parameters were as follows: tube voltage 120–140 kV, tube current with automated dose modulation 60–440 mA/slice, collimation 64×0.625, pitch 0.984:1, rotation time 0.5 s, coverage speed 78 mm/s, field of view (FOV) 50 cm, and images with a transverse pixel size of 0.625, and a slice thickness of 3.75 mm reconstructed in

axial, coronal, and sagittal planes [11]. Different PET reconstruction settings were tested in this study and will be discussed in the following sections.

PET/MRI Imaging

After the PET/CT examination, the patient was moved to the adjacent PET/MRI room, with a mean interim time of 15 min for brain scans (respectively 30 min for the whole-body scans). The brain scans lasted for 20 min while the whole-body scans were acquired with 4 min per bed position. The reason for this acquisition times was to expose both systems to the same amount of emitted counts (see also "Data Processing").

Patients were positioned in supine position with the arms down. Before the acquisition of the PET data, a whole-body MR localizer scan was performed in craniocaudal direction. The standard patient radiofrequency (RF) coil setup always included a 19-channel head and neck unit, 16-channel upper and lower anterior arrays, and a 19-channel central matrix array (GE Healthcare, Waukesha, WI, USA).

Next, the three-dimensional emission scan was planned and started. The operator is prompted for setting anatomical boundaries. The default number of bed positions was six, from the vertex of the skull to the mid-thighs, but adjustable to meet every patient's body length. During PET scanning, a multi-station whole-body, 3D, dual-echo, RF-spoiled gradient recalled echo (SPGR) sequence (LAVA-FLEX) was acquired for the purpose of PET attenuation correction. With the two echoes, in-phase and out-of-phase images were acquired and water-only and fat-only images were calculated automatically [12, 13]. The sequence parameters were repetition time (TR) 4.056 ms, echo time (TE) out-of-phase 1.116 ms, (TE) in-phase 2.232 ms, flip angle (FA) 12°, field of view (FOV) 500×375 mm (frequency×phase), acquisition matrix 256×128, 1 slab with 64×5.2-mm thick axial slices, voxel size 1.95×2.93 mm, and 1 average. For attenuation correction, the system only uses the body coil. The total acquisition time per bed position was 18 s. The MR-based attenuation correction algorithm uses an anatomical atlas for the patient's head region and an air, lung, and continuous fat/water segmentation for the other body regions [11].

Data Processing

Our goal was to expose both systems to the same amount of emitted signal in order to assess clinically their sensitivity performance in conditions as similar as possible. Administering a second tracer injection to the patient was not possible, so we opted to adjust the acquisition times to account for tracer decay between the acquisitions. This had to be done retrospectively due to the unpredictable nature of the time delay between scans.

The acquisition times were manually adjusted by unlisting the list mode data, creating sinograms that could then be compared for each acquisition time. The decay integrals for the whole examination duration were extracted and adjusted so that the PET/MRI and PET/CT emission data were equivalent. The two resulting sinograms are then representative of a situation in which the patient has received the same injected activity for each scan.

For the brain scans, the original scan duration times were 10 and 20 min for PET/CT and PET/MRI, respectively. After correcting for the decay integrals so that they were equivalent, we calculated that PET/MRI acquisition time matched the PET/CT acquisition time with a reduced scan time of an average of 13:51±00:40 min.

For the whole-body scans, the original acquisition times were 16 and 24 min for PET/CT and PET/MRI (2 min/bed for 8 beds, 4 min/bed for 6 beds), respectively. As explained above, the PET/MRI list mode data were shortened to be equivalent to the PET/CT. The resulting PET/MRI list modes were on average 03:26 ±00:25 min/bed.

Our next step was to reduce both PET/CT and PET/MRI acquisition times in fixed time frames to simulate how the systems respond to lower count rates and to compare image quality step by step with reduced acquisition times.

For the brain scans, we unlisted the emission data for 8:00, 6:00, 5:00, 4:00, and 3:00 min for PET/CT and the corresponding equivalent times for PET/MRI were 11:06 ±0:35, 8:18±0:35, 6:54±0:30, 5:30±0:30, and 4:07±0:30. For the whole-body scans, we unlisted the emission data for 2:00, 1:40, 1:20, 1:00 min/bed, and 00:40, 00:30 s/bed for PET/CT and the corresponding equivalent times for PET/MRI were 03:26, 02:50, 02:14, 01:38, 01:08, and 00:53 ±00:25.

Reconstruction methods were carefully selected to be as similar as possible for both scanners. Thus, equivalent rather than identical settings were required because the scanners have different geometries, so parameters like z-axis resolution and transaxial FOV vary and the reconstructed images would not fit for reliable comparison. This is due to the different detector geometry between the two systems. The LYSO crystals on both systems share the same thickness but the PET/MRI has a slight advantage having smaller crystals in both transaxial and axial directions which leads to improved image resolution (*e.g.*, transaxial spatial resolution for PET/CT is 4.7 mm full width at half maximum (FWHM) [9] while for PET/MRI is 3.9 mm FWHM [8] at 1 cm from FOV center). Both emission data were iteratively reconstructed (VUE Point FX), TOF-OSEM (3 iterations, 16 subsets), reconstruction matrix 256×256, with point-spread-function, corrected in a standardized way (random, scatter, and attenuation), 30 and 60 cm transaxial FOV for the brain and whole-body, respectively, Gaussian post-filter 2.0 mm. In order for the comparison to be the most reliable, no z-axis filter was applied since longitudinal resolution between the scanners varied.

Quantitative Evaluation

Two-dimensional regions of interest (2D-ROIs) with sizes of 634.5 and 134.6 mm^2 were drawn in the liver (on coronal plane) and in the white matter of the brain (on axial plane), respectively, at the same position for each of the images for all acquisition times, for both PET/CT and PET/MRI, and for all patients. Here, it should be noted that the 2D-ROIs both in the liver and in the brain were drawn in healthy and not pathological tissue. Mean signal values from all 2D-ROIs were extracted and compared.

Clinical Evaluation

The acquired brain and whole-body PET/CT and PET/MRI images were sent to a dedicated review workstation (Advantage Workstation 4.6, GE Healthcare, Milwaukee, WI), which allows for the simultaneous review of the PET/CT and PET/MRI images. The images were reviewed clinically and compared by a dually-board-certified radiologist/nuclear medicine physician and a radiologist with substantial experience in PET/CT in consensus. Differences in the images were noted and assessed using a 4-point scale for the scoring of image quality (4=excellent, 3=good, 2=acceptable, 1=insufficient), image sharpness (4=perfectly sharp, 3=good, 2=acceptable, 1=blurry), and noise (4=no noise, 3=slight, 2=considerable, 1=unacceptable) while a 3-point scale is used for the artifacts (3=no artifact, 2=slight, 1=considerable).

Statistical Evaluation

To assess the correlation between PET/CT and PET/MRI for the liver and the brain, trend lines were drawn for the cluster of the brain and for the cluster of the liver and the coefficients of determination were obtained (Fig. 1, see Suppl. Table 1). Each cluster consists of five sub-clusters corresponding to the number of the patients. An additional condition forced the linear regression to cross the origin because zero uptake corresponds to zero standardized uptake value (SUV) in both scanners.

Results

Quantitative Evaluation

The results of the quantitative evaluation on regions of interest defined on the liver and white matter are shown in Fig. 1. The average SUV in each ROI is represented by a point in the scatter plot, with PET/CT SUV represented in the x-axis and PET/MRI SUV on the y-axis. Connected sub-clusters of points represent, for each patient, corresponding measurements on a series of reconstructions with decreasing acquisition time (hence mimicking the behavior of dose reduction). Thus, each sub-cluster consists of six points

representing the SUV value for each acquisition time. Notice how the obtained average uptake values for individual patients are consistent between reconstructions and display similar variability in the PET/CT and PET/MRI axes. As expected, there is clear organization in two separate, compact clusters for liver and white matter measurements. Uptake values in the brain are estimated to be higher in PET/MRI compared to PET/CT, whereas uptake values measured in the liver are estimated to be lower. Notice that tracer decay has been corrected for in this comparison.

The coefficient of determination (R^2) between PET/CT and PET/MRI for the liver cluster has a value of 0.61703 and for the brain cluster a value of 0.95895, showing that there is strong correlation between PET/CT and PET/MRI brain SUVs while there is a good correlation for the liver SUVs.

Clinical Evaluation

The reconstructed PET/CT and PET/MRI datasets were qualitatively evaluated. A set of anatomical landmarks were scored for each patient and acquisition time. Table 1 and supplementary Tables 2 to 4 summarize these results, averaged over all patients. Table 1 shows the overall image quality scores (see sample brain and whole-body images in Figs. 6 and 7, respectively), both for brain and whole-body studies. PET/MRI and PET/CT scores are provided in pairs, in decreasing acquisition time steps. The corresponding tables for the image sharpness (Suppl. Table 2), artifacts (Suppl. Table 3), and noise (Suppl. Table 4) are provided as Supplementary Material. There was a statistically significant difference for body imaging in image quality ($p<0.001$), image sharpness ($p<0.001$), and noise ($p<0.001$) while there was no significant difference for artifacts ($p>0.05$), showing a superiority of PET/MRI *versus* PET/CT. Remarkably it can be noticed that the differences in body imaging can be seen in all categories and at all time point, except in artifacts.

However, no significant difference was noticed in brain imaging where both imaging methods showed comparable results ($p>0.05$) (Figs. 2, 3, 4, and 5).

Discussion

To our knowledge, this is one of the first evaluations on image quality comparing standard TOF-PET/CT and simultaneous TOF-PET/MRI with different imaging times. We have shown that the PET component of the PET/MRI provides higher overall image quality as perceived by a clinical reader compared to PET/CT. Furthermore, the quantitative evaluation of brain and whole-body studies showed that PET/MRI and PET/CT do not calculate equivalent SUV-values. While this can be partly justified by bio-redistribution of the tracer, (as seen in Fig. 3 of [19]), there is still a big SUV value difference for the ROI placed in the liver around 35 to 40 %, while there is approximately
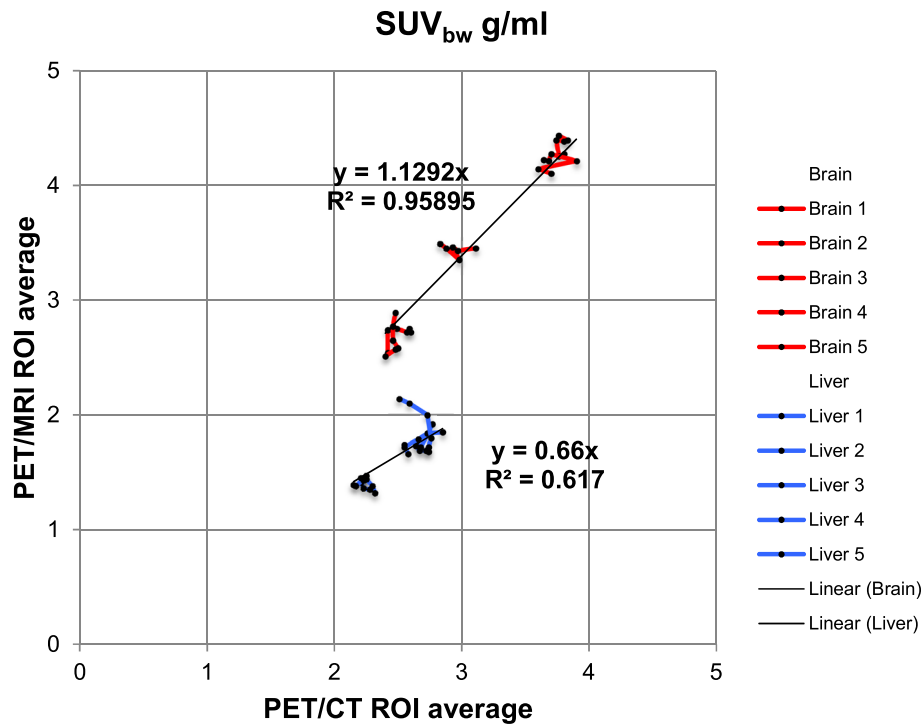
SUV$_{bw}$ g/ml

Fig. 1 PET/CT average compared to the PET/MRI one for the brain (white matter) 2D-ROI and whole body (liver) 2D-ROI for all patients and all reconstruction times. The *black dots* indicate the value of the 2D-ROIs, and the *red* and *blue lines* indicate the brain sub-clusters (one for each patient) and the whole-body sub-clusters (one for each patient), respectively.

Table 1. Image quality scores for all anatomical regions assessed for all equivalent acquisition times for both PET/CT and PET/MRI, averaged over all five patients, using the 4 point scale mentioned in "Procedures"

| General image quality scores	PET/CT	PET/MRI	PET/CT	PET/MRI	PET/CT	PET/MRI	PET/CT	PET/MRI	PET/CT	PET/MRI	PET/CT	PET/MRI
	10 min		8 min		6 min		5 min		4 min		3 min	
Brain												
Anterior limb of internal capsule	4	3.8	3.8	3.6	3.8	3.8	3.6	3.8	2.8	2.8	2.8	2.8
Posterior limb of internal capsule	4	4	4	3.8	3.8	3.6	3.6	3.4	3	2.8	2.6	2.8
Cerebellar vermis	3.4	3.6	3.4	3.4	3.2	3.2	2.6	2.8	2.4	2.2	2.2	2
Dentate nucleus	4	4	3.8	3.6	3.2	3.2	2.8	2.8	2.6	2.6	2.2	2
Gray/white matter												
Cerebellar	3.8	3.8	3.6	3.8	3.4	3.4	2.8	3	2.4	2.2	2.2	2.2
Frontal	4	4	4	4	3.8	3.6	3.2	3.4	2.6	2.6	2.2	2.4
Insular	4	4	4	4	3.8	3.8	3.4	3.2	2.8	2.8	2.4	2.6
Occipital	4	4	4	4	3.6	3.6	3.2	3	2.6	2.6	2	2.2
Parietal	4	4	4	4	3.8	3.6	3.2	3	2.6	2.6	2.4	2.6
Temporal	4	4	4	4	3.8	3.8	3.4	3.4	2.8	2.8	2.6	2.8
Nucleus ruber	3.8	4	3.6	3.8	3	3.2	2.8	2.8	2.4	2.6	1.8	1.8
Optic nerve	2.6	2.6	2.6	2.6	2.4	2.4	1.6	1.8	1.4	1.4	1	1.2
Putamen *vs.* globus pallidus	4	4	3.8	3.6	3.4	3.4	2.6	2.6	2.4	2.6	2	2
Tectum	3.6	3.8	3.4	3.6	2.8	3	2.6	2.8	2.2	2.4	1.6	1.6
	2 min /bed		1:40 min/bed		1:20 min/bed		1:00 min/bed		40 s/bed		30 s/bed	
Whole body												
Blood pool (RA)	3.6	4	3.6	4	3.2	3.6	2.8	3.4	1.8	3	1.6	2.4
Bone marrow	3.2	3.8	2.8	3.8	2.2	3.2	2	2.8	1.2	2.2	1	1.6
Heart (LV-muscle)	3.6	3.8	3.6	3.8	3.4	3.6	3	3.4	2.2	3	1.8	2.6
Liver (right lobe)	3.6	4	3	3.8	3	3.4	2.2	2.8	1.4	2.4	1.2	1.6
Lung	3.2	4	3.2	3.8	2.8	3.2	2.4	3	1.6	2.2	1.4	1.8
Muscle	3.2	4	2.8	3.6	2	3.2	1.8	2.8	1.6	2.6	1.2	1.6
Spleen	3.4	3.8	3	3.6	2.6	3.4	2.2	3	1.4	1.8	1.4	1.2
Subcutaneous fat	3.6	4	3	4	2.4	3.6	2	3	1.6	2.6	1.2	2
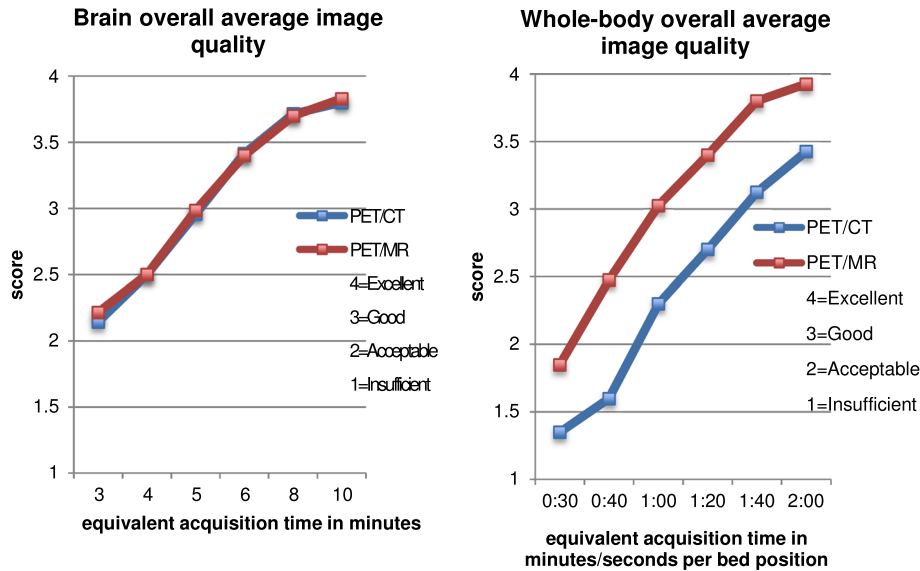
Fig. 2 Brain and whole-body image quality scores averaged over all anatomical regions and all five patients for equivalent acquisition times for both PET/CT and PET/MRI.

a 15 % SUV value difference for the ROI placed in the white matter (see Suppl. Table 1).

In this study, we assessed the PET performance of both PET/CT and PET/MRI scanners for five brain and five whole-body studies. The PET/MRI acquisition time was retrospectively adjusted for each patient to account for tracer decay since the start of the PET/CT acquisition. This ensured that the reconstructed images used for the evaluation offered a fair comparison where both systems had been exposed to equivalent amounts of the emitted signal (Figs. 6 and 7).

Additionally, the acquired datasets were then used to simulate multiple acquisitions of decreasing scan time. This was used to evaluate the performance of the PET component at gradually lower count statistics, providing an estimate of the dose reduction capabilities of the new scanner.

Objective evaluation of the reconstructed image was based on region of interest analysis. 2D-ROIs were drawn in the white matter of the brain and in the liver and the average uptake values measured. As expected, the results show that there is not always a quantitative equivalence between PET/CT and PET/MRI uptake values. This could,
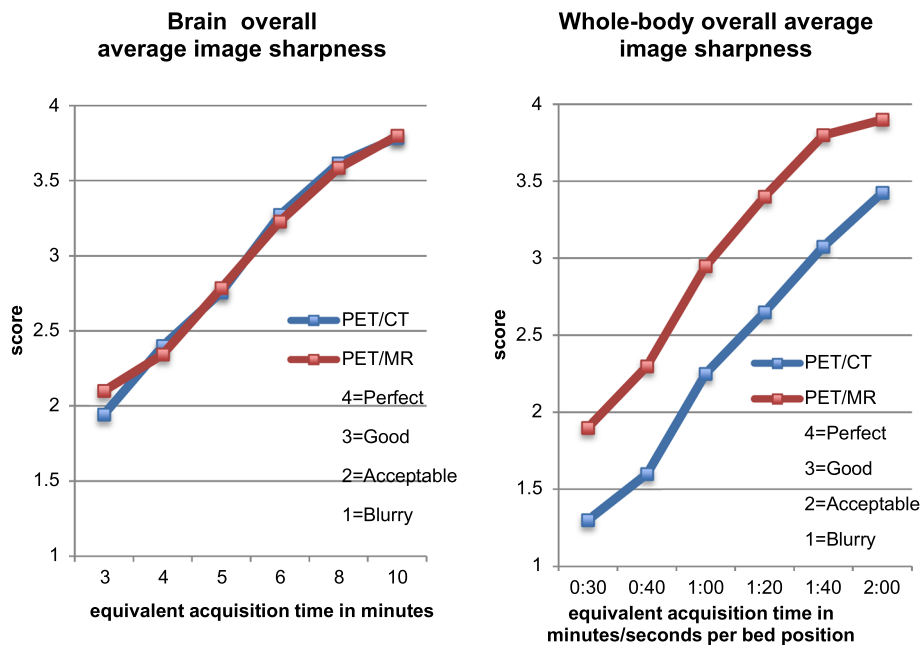

Fig. 3 Brain and whole-body image artifact scores averaged over all anatomical regions and all five patients for equivalent acquisition times for both PET/CT and PET/MRI.
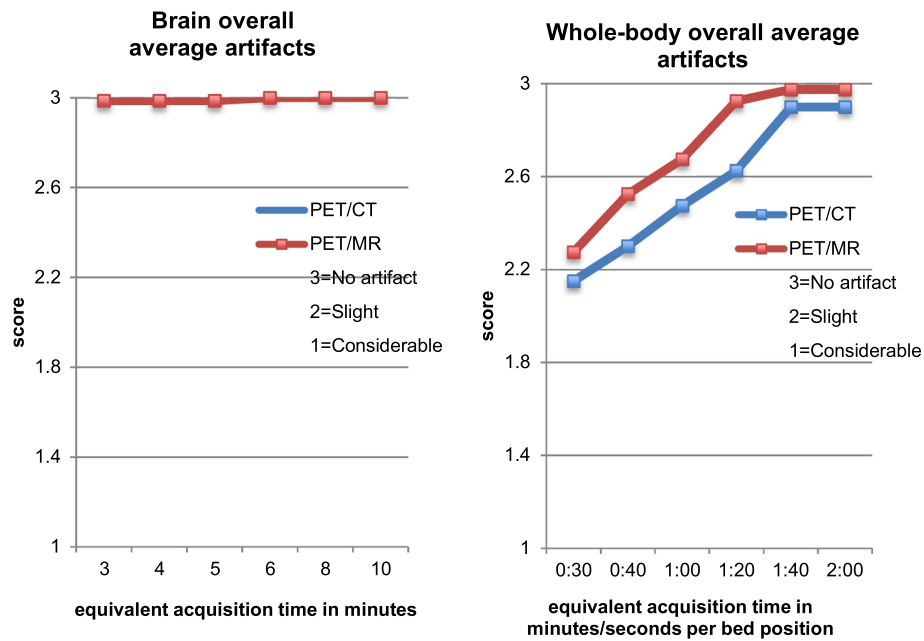
Fig. 4 Brain and whole-body image sharpness scores averaged over all anatomical regions and all five patients for equivalent acquisition times for both PET/CT and PET/MRI.

of course, severely limit the compatibility of these modalities in follow-up studies. On the other hand, biological redistribution of the tracer during the time between PET/CT and PET/MRI acquisitions can partly explain the SUV differences found in liver measurement, as previously reported in [14]. Furthermore, Fig. 1 shows a clearly consistent behavior for liver and white matter groups. As a matter of fact, the Signa PET/MRI system uses different attenuation estimation methods for the head (atlas-based) and the body (4-class segmentation). Higher estimation of brain SUVs may therefore be attributed to insufficient anatomical accuracy

of the atlas or insufficient constraints in the elastic registration (*e.g.,* skull thickening). The lower estimation of the liver SUVs can be due to the attenuation of anterior upper and lower coils not being accounted for (only head/neck and bed coils are corrected for attenuation due to fixed position regardless of patient size), or to minor inaccuracies in the attenuation coefficients assigned to the segmented tissue classes. Further investigation is required that can ultimately lead to a fine-tuning of MRAC.

Clinical evaluation shows equivalent performance for brain studies. This is coherent with literature [9, 15]. Most of
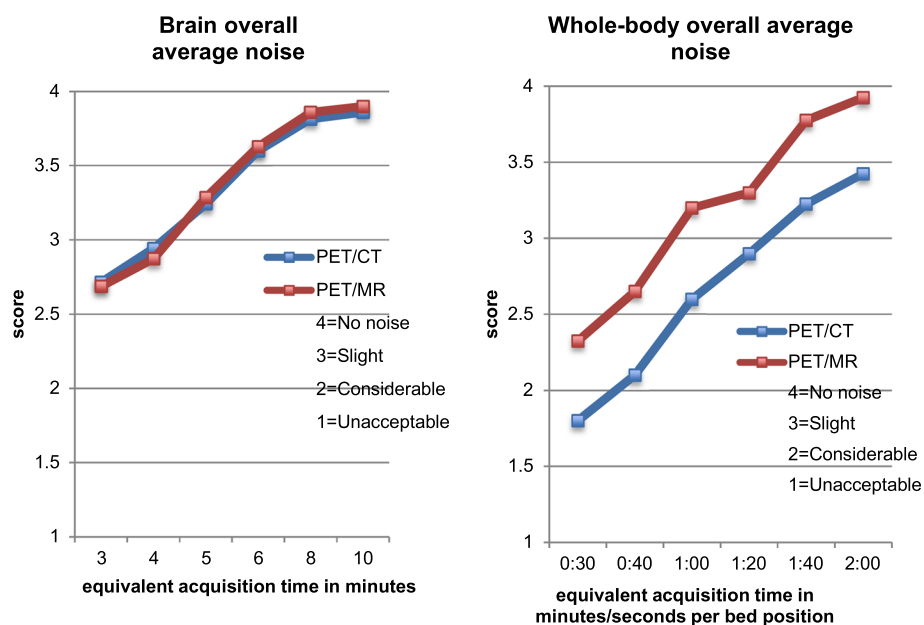
Fig. 5 Brain and whole-body image noise scores averaged over all anatomical regions and all five patients for equivalent acquisition times for both PET/CT and PET/MRI.
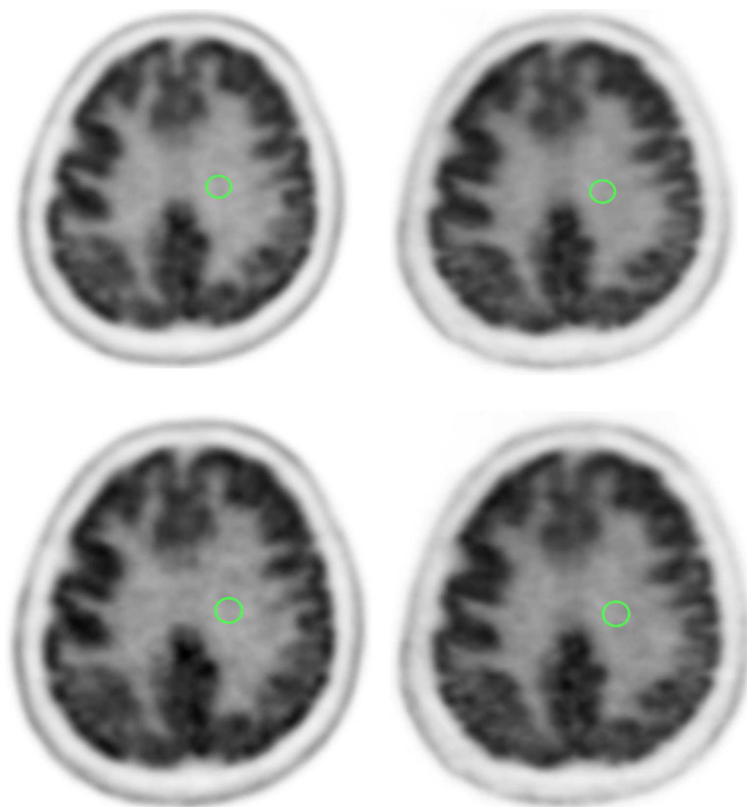
Fig. 6 *Upper row*: PET/CT and PET/MRI original acquisition time brain images with the drawn 2D ROI (*green circle*) in white matter from one subject. *Lower images*: PET/CT and PET/MRI with 5 min acquisition time brain images with the drawn 2D ROI (*green circle*) in the white matter.

the FOV of PET/MRI is not used, so sensitivity cannot be taken advantage of and lead to improved image quality. This is due to the fact that the slice-wise increase of sensitivity at the isocenter is not large enough to make a noticeable difference in brain images. Another reason for this observation could be that the image quality in brain PET/CT images is already very good and that improvements due to increased counts are hard to distinguish.

The image quality, sharpness, artifacts, and noise for PET/CT and PET/MRI for all acquisition times were clinically assessed and scored.

Clinical evaluation indicated better performance for the whole-body studies. In this case, the bigger FOV of the PET/MRI is fully used so higher sensitivity provides significantly improved image quality compared to the PET/CT.

As a consequence of the improved quality, there is potential for dose or acquisition time reduction in whole-body studies. Taking the general image quality diagram and going with a scoring of acceptable quality, calculating the acquisition time values based on the horizontal shift of the two curves on the plot, PET/MRI can provide a 37 % (32/51 s for PET/MRI and PET/CT, respectively) reduction in dose or acquisition time, result that is coherent with previous data [16]. There are studies that have suggested further dose reduction in PET/MRI with prolonging the acquisition time [17] since MRI usually takes more time anyway, but this depends on the clinical indication and the type of

examination. In any case, this is promising and should be put to the test in a future study. On the contrary, what we have shown is that taking advantage of the higher geometric efficiency (factor of ~2 for PET/MRI compared to PET/CT) and higher detector sensitivity of PET/MRI [10] dose reduction can be achieved in PET/MRI with keeping the acquisition times fixed. For a standard patient, this reduction in injected activity means that the patient's effective dose can be reduced by 1.75 mSv. Instead of the standard injected activity of 250 MBq, the patient can be injected with 157 MBq that will deliver 3 mSv instead of 4.75 mSv (0.019 mSv/MBq for standard patient size [18]). From a radiation protection perspective, this is consistent with the ALARA principle [19] for keeping the exposure of the patient to radiation as low as possible while at the same time obtaining sufficient image quality.

Conclusion

In this study, we compared the PET performance of PET/MRI and PET/CT for various acquisition times. The quantitative results show differences for both brain and whole-body studies. These differences may be explained by bio-redistribution [20]. However, a preliminary check suggests that the measured differences are not fully accounted for by the referenced models [20]. Hence, other causes must be investigated (*e.g.*, minor deviations of patient
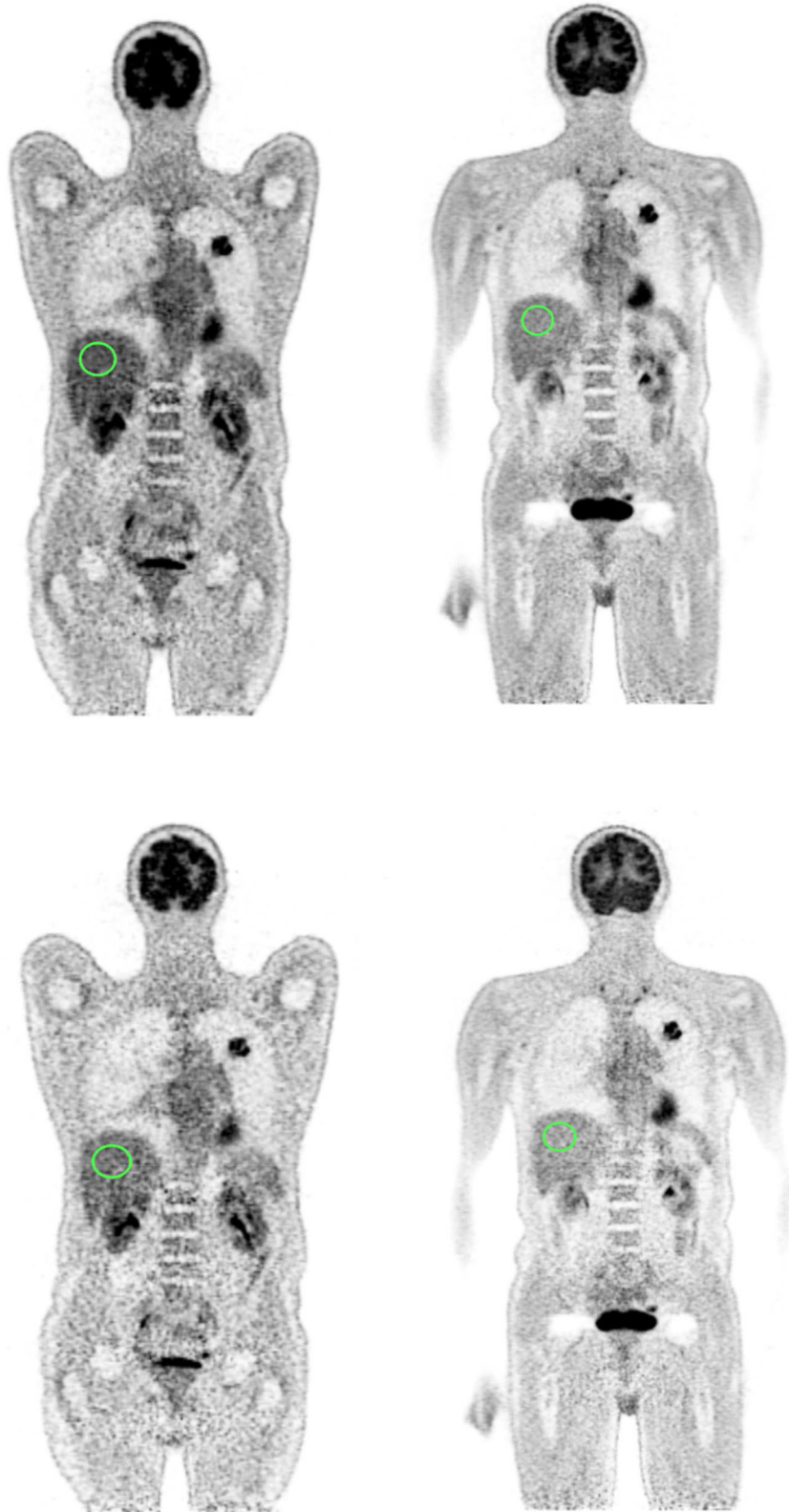
Fig. 7 *Upper images*: PET/CT and PET/MRI original acquisition time whole body images with the drawn 2D ROI (*green circle*) on the coronal plane in the liver. *Lower images*: PET/CT and PET/MRI with 1 min per bed frame acquisition time whole body images with the drawn 2D ROI (*green circle*) on the coronal plane in the liver.

attenuation from the 4-tissue-class model or reconstruction convergence differences). The clinical assessment of the

brain studies indicate that there is no significant difference between the two scans while for the whole-body studies the

image quality and the sharpness are constantly higher for PET/MRI with at the same time lower levels of noise and same levels of artifacts compared to PET/CT. This overall higher image quality, due to higher geometric efficiency and detector sensitivity, suggests that the acquisition time or injected activity can be reduced by at least 37 % on the PET/MRI scanner.

Ethical Approval. All procedures performed in studies involving human participants were in accordance with the ethical standards of the institutional and/or national research committee and with the 1964 Helsinki declaration and its later amendments or comparable ethical standards.
Informed consent was obtained from all individual participants included in the study.

Conflict of Interest. Patrick Veit-Haibach received IIS Grants from Bayer Healthcare, Siemens Medical Solutions, Roche Pharma and GE Healthcare, and speaker fees from GE Healthcare. The authors declare no other conflict of interest.

Electronic Supplementary Material

Below is the link to the electronic supplementary material.ESM 1(PDF 213 kb)

References

1. Townsend DW (2008) Combined positron emission tomography-computed tomography: the historical perspective. Semin Ultrasound CT MR 29:232–235
2. Sauter AW, Wehrl HF, Kolb A et al (2010) Combined PET/MRI: one step further in multimodality imaging. Trends Mol Med 16:508–515
3. Pichler BJ, Wehrl HF, Kolb A, Judenhofer MS (2008) Positron emission tomography/magnetic resonance imaging: the next generation of multimodality imaging? Semin Nucl Med 38:199–208
4. Pichler BJ, Kolb A, Nagele T, Schlemmer HP (2010) PET/MRI: paving the way for the next generation of clinical multimodality imaging applications. J Nucl Med 51:333–336
5. Delso G, Furst S, Jakoby B et al (2011) Performance measurements of the Siemens mMR integrated whole-body PET/MR scanner. J Nucl Med 52:1914–1922
6. Delso G, Martinez MJ, Torres I et al (2009) Monte Carlo simulations of the count rate performance of a clinical whole-body MR/PET scanner. Med Phys 36:4126–4135
7. Catana C, Drzezga A, Heiss WD, Rosen BR (2012) PET/MRI for neurologic applications. J Nucl Med 53:1916–1925
8. Levin C, Glover G, Deller T et al (2013) Prototype time-of-flight PET ring integrated with a 3T MRI system for simultaneous whole-body PET/MR imaging [abstract]. J Nucl Med 54(Supplement 2):148
9. Bettinardi V, Presotto L, Rapisarda E et al (2011) Physical performance of the new hybrid PETCT Discovery-690. Med Phys 38:5394–5411
10. Levin C, Deller T, Peterson W et al (2014) Initial results of simultaneous whole-body ToF PET/MR [abstract]. J Nucl Med 55(Supplement 1):660
11. Stolzmann P, Veit-Haibach P, Chuck N et al (2013) Detection rate, location, and size of pulmonary nodules in trimodality PET/CT-MR: comparison of low-dose CT and Dixon-based MR imaging. Invest Radiol 48:241–246
12. Dixon WT (1984) Simple proton spectroscopic imaging. Radiology 153:189–194
13. Bley TA, Wieben O, Francois CJ et al (2010) Fat and water magnetic resonance imaging. J Magn Reson Imaging 31:4–18
14. Cheng G, Alavi A, Lim E, Werner TJ, Del Bello CV, Akers SR (2013) Dynamic changes of FDG uptake and clearance in normal tissues. Mol Imaging Biol 15:345–352
15. Deller T, Grant A, Khalighi MM, et al. (2014). PET NEMA Performance Measurements for a SiPM-Based Time-of-Flight PET/MR System [abstract]. IEEE NSS/MIC:M08-6
16. Marcelo Queiroz SW, von Schulthess G, Delso G, Veit-Haibach P (2014) Clinical image quality perception and corresponding NECR measurements in PET. J Nucl Med 55(Suppl 1):1
17. Oehmigen M, Ziegler S, Jakoby BW et al (2014) Radiotracer dose reduction in integrated PET/MR: implications from national electrical manufacturers association phantom studies. J Nucl Med 55:1361–1367
18. Harding K (1991) ICRP 60 and future legislation. Nucl Med Commun 12:753–755
19. Lundell G, Hall P, Holm LE (1992) [Follow the ALARA principle]. Lakartidningen 89:3917
20. Laffon E, Adhoute X, de Clermont H, Marthan R (2011) Is liver SUV stable over time in (18)F-FDG PET imaging? J Nucl Med Technol 39:258–263